Supporting Information for

Weakened and Irregular Miocene Climate Response to Orbital Forcing compared to the modern day

Yurui Zhang[1*], Jilin Wei[2,3], Zhen Li[1], Nan Dai[1], Weipeng Zheng[2,3,5], Qiuzhen Yin[6], Agatha M. de Boer[6], Zhengguo Shi[7,8], Lixia Zhang[2]

[1]State Key Laboratory of Marine Environmental Science, College of Ocean & Earth Sciences, Xiamen University, Xiamen, China

[2]State Key Laboratory of Earth System Numerical Modeling and Application, Institute of Atmospheric Physics, Chinese Academy of Sciences, Beijing, China

[3]College of Earth and Planetary Sciences, University of Chinese Academy of Sciences, Beijing, China

[4]Earth System Numerical Simulation Science Center, Institute of Atmospheric Physics, Chinese Academy of Sciences, Beijing, China

[5]Earth and Climate Research Center, Earth and Life Institute, Université catholique de Louvain, Louvain-la-Neuve, Belgium

[6]Department of Geological Sciences, Bolin Centre for Climate Research, Stockholm University, Sweden

[7]State Key Laboratory of Loess Science, Institute of Earth Environment, Chinese Academy of Sciences, Xi'an, China

[8]Institute of Global Environmental Change, Xi'an Jiaotong University, Xi'an, China

Correspondence to: Yurui Zhang (yuruizhang@xmu.edu.cn)

Contents of this file

Text S1. FGOALS-g3 climate model

FGOALS-g3 is a fully coupled general circulation model representing the latest generation of climate system model used in CMIP6 (Li et al., 2020). The atmospheric (GAMIL3) and land (CAS-LSM) components have a horizontal resolution of 2 °with 26 vertical layers (Li et al., 2020; Xie et al., 2020). The ocean (LICOM3) and sea ice (CICE) components use a tripole grid with 360 × 218 horizontal grids and 30 vertical layers (Lin et al., 2022). These components are coupled through the flux coupler CPL7, which enables the exchange and synchronization of the climate variables (Anthony et al., 2011). Model evaluations indicate improved simulating of atmospheric and ocean dynamics compared to its previous versions (Li et al., 2020; Lin et al., 2022). FGOALS-g3 has been used extensively for present-day simulation (Lin et al., 2022; Wang et al., 2020) and paleoclimate studies, including the Miocene to mid-Holocene (Wei et al., 2023; Zheng et al., 2020). Further details are available in Li et al. (2020) and Wei et al. (2023).

Text S2. Model performance evaluation

To assess the model's ability to simulate climate seasonality and spatial patterns, we compared the PI simulation with other CMIP5 climate models and with ERA5 reanalysis data, focusing on JJA and DJF temperatures (Fig. S3). On average, the PI simulation shows the same pattern of seasonality and similar degree seasonality as the multi-model mean and ERA5 data (Fig. S3). The absolute value is approximately 2℃ cooler than in ERA5, partially due to anthropogenic warming (Gillett et al., 2021), as the PI simulation represents conditions around 1850 BP, while ERA5 reflects a more recent, warmer climate.

Spatially, the PI simulation effectively reproduces the 10℃ and 25℃ isothermal lines for boreal summer (JJA) and winter (DJF), closely matching multi-model mean and ERA5. However, the slightly larger contour areas in ERA5 suggest a minor cold bias in the PI simulation, consistent with the global mean temperature difference noted above, likely enhanced by polar amplification. A more pronounced discrepancy appears in Arctic Eurasia during winter, where the PI simulation and mult-model are colder (Fig. S3), likely due to excessive sea ice thickness—a common issue in climate models (Davy and Outten, 2020). This Arctic cold bias enhances seasonal temperature contrast over northwest Eurasia, a feature also observed in many CMIP6 models (Fan et al., 2020). Despite these differences, the PI simulation reasonably captures seasonal temperature variations in both magnitude and spatial pattern.

Table S1. Model simulation setup

Simulation	Geography Setting	pCO_2(ppm)	Orbital forcing			Duration of simulation (yrs)	TOA* (W/m^2)	GMAT** (°C)
			Eccentr	Obliquity (rad)	Long. Perih			
PI	Modern	280	0.0167	0.4091	102.040 °	1700	-0.04	15.61
PIorbmax			0.0508	0.4208	281.387 °	300	0.05	15.75
PIorbmin			0.0599	0.3983	68.158 °	300	-0.17	15.71
MI-3x	Miocene (~15Ma)	840	0.0167	0.4091	102.040 °	1700	0.34	22.32
MIorbmax			0.0508	0.4208	281.387 °	400	0.28	22.47
MIorbmin			0.0599	0.3983	68.158 °	400	0.30	22.58

TOA*: Top-of-Atmosphere (TOA) radiation imbalance; GMAT**: Global Mean Air Temperature.

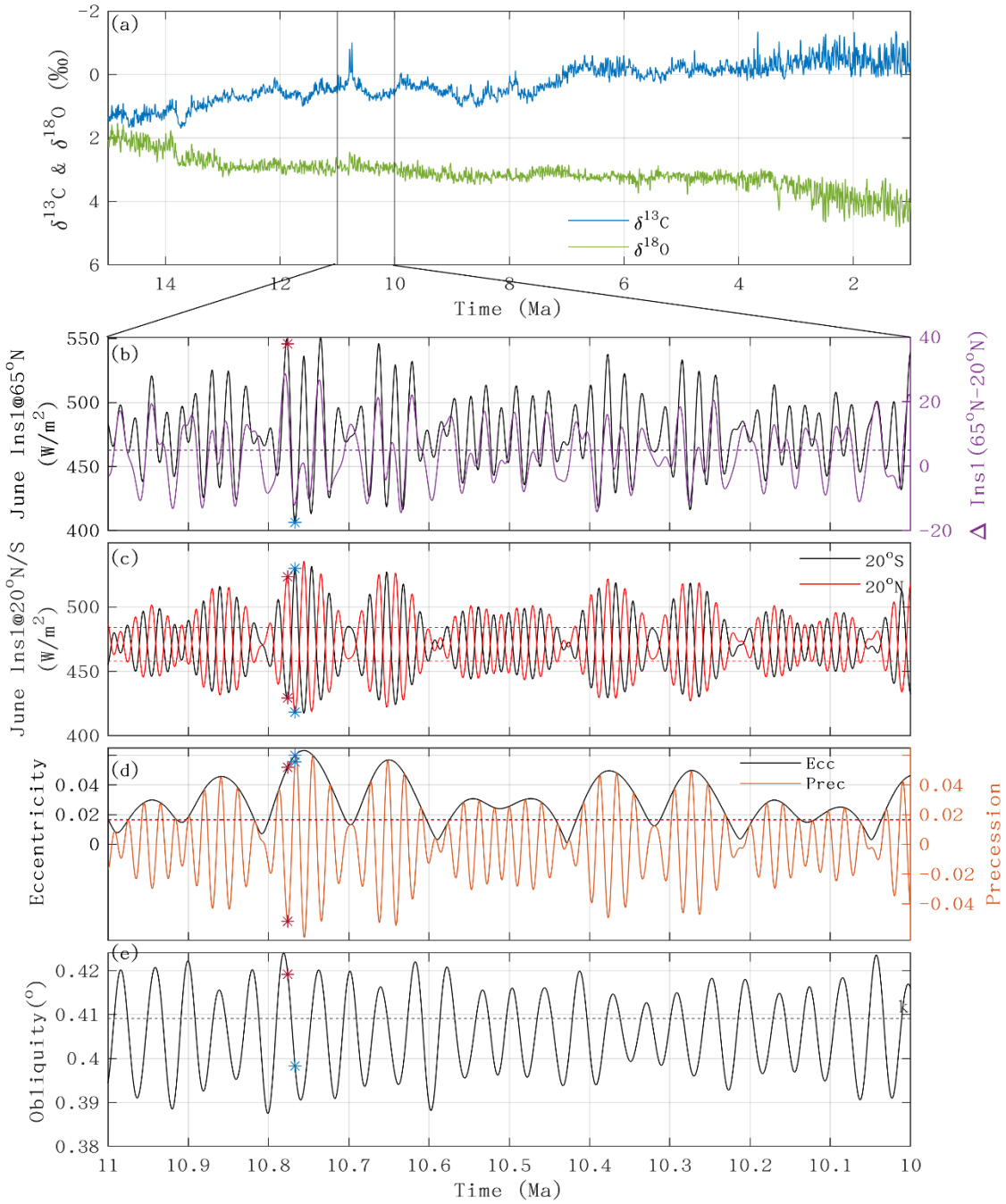

Figure S1 Orbital parameters setup and their effects on insolation. (a) δ¹⁸O and δ¹³C records (Westerhold et al., 2020), (b) insolation at 65 ℕ and difference from 20 ℕ (Laskar, 2010). (c) June insolation at 20 ℕ/S. (d) Eccentricity and Precessions showing as e*sin(longitude of Perihelion). (e) Obliquity in rad. Dash lines mark the modern day value used in the baseline experiments. Orange and blue stars indicate the corresponding setup for the orbmax and orbmin experiments.

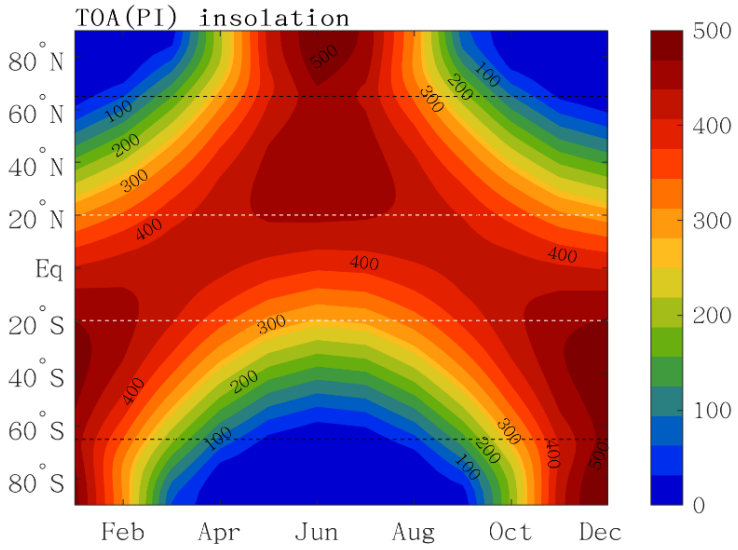

Figure S2. TOA insolation (W/m^2) in the baseline simulation, with white and black dashed lines indicating the location of 20 ℃N/Sand 65 ℃N/S which insolation is given in Fig. S1.

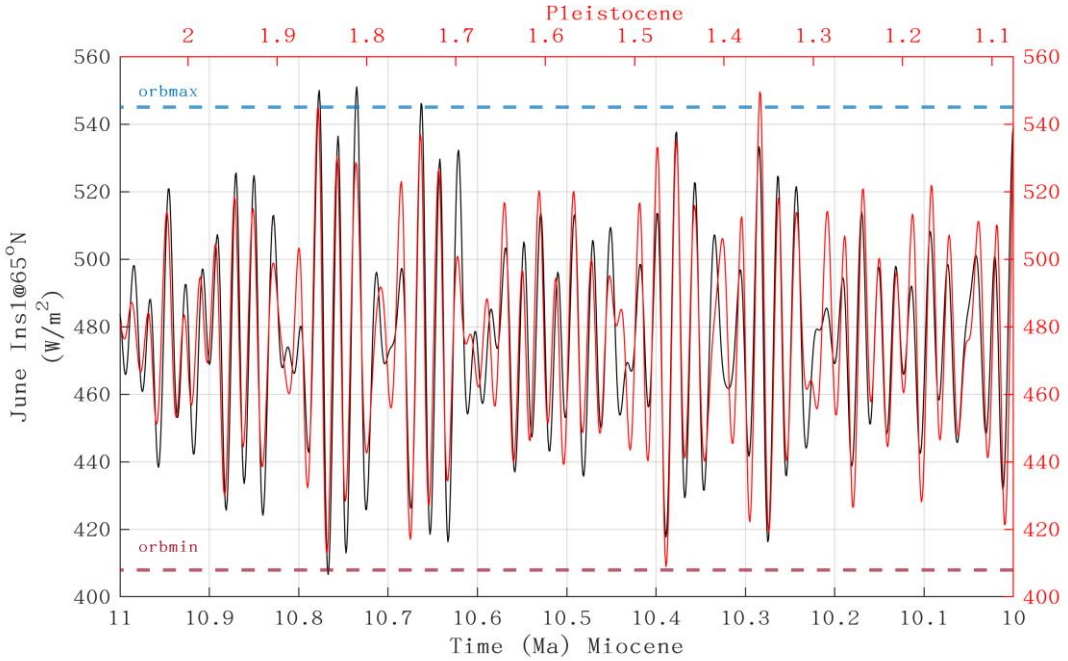

Figure S3. Comparison of the time series of June insolation (W/m^2) at 65 ℃N between the Miocene (black) and Pleistocene (red).

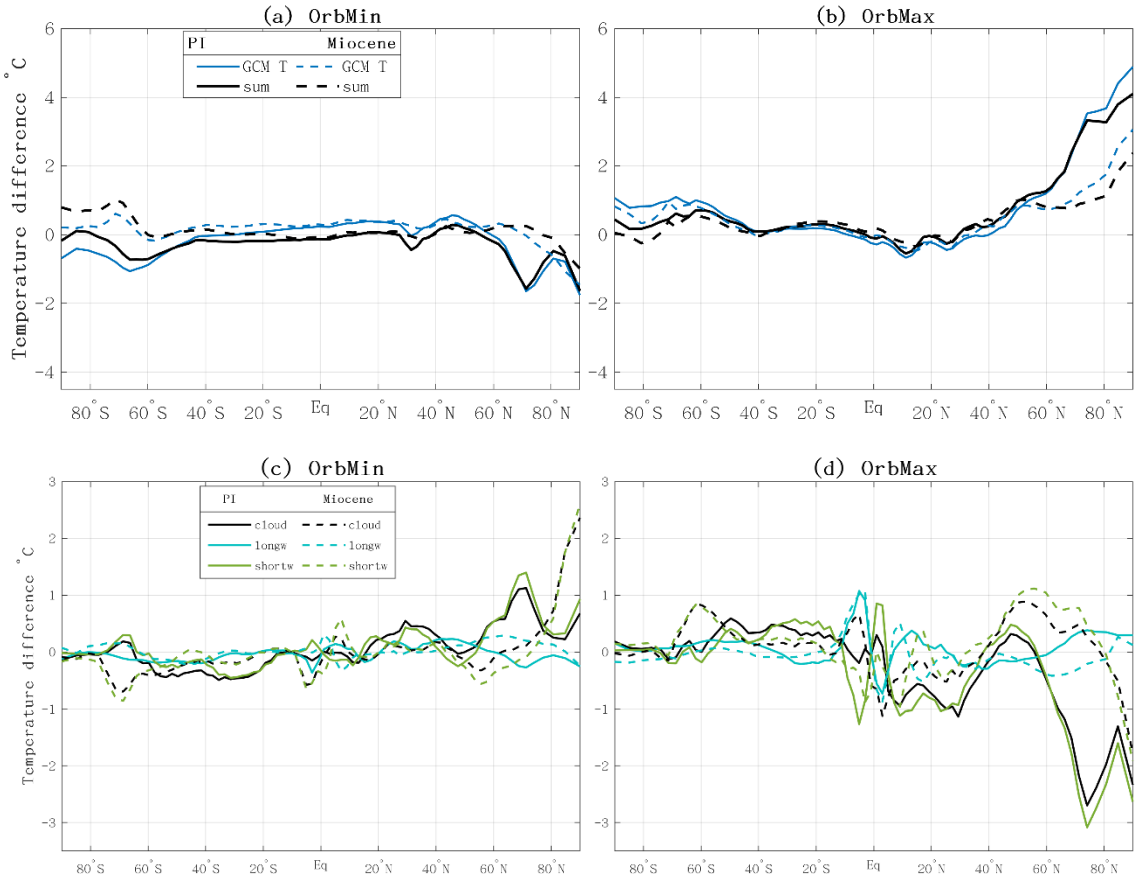

Figure S4. Comparison of the sum of EBA components with the GCM results for orbmin (a) and orbmax (b), and decomposition of cloud components into longwave and shortwave contributions for orbmin (c) and orbmax (d).

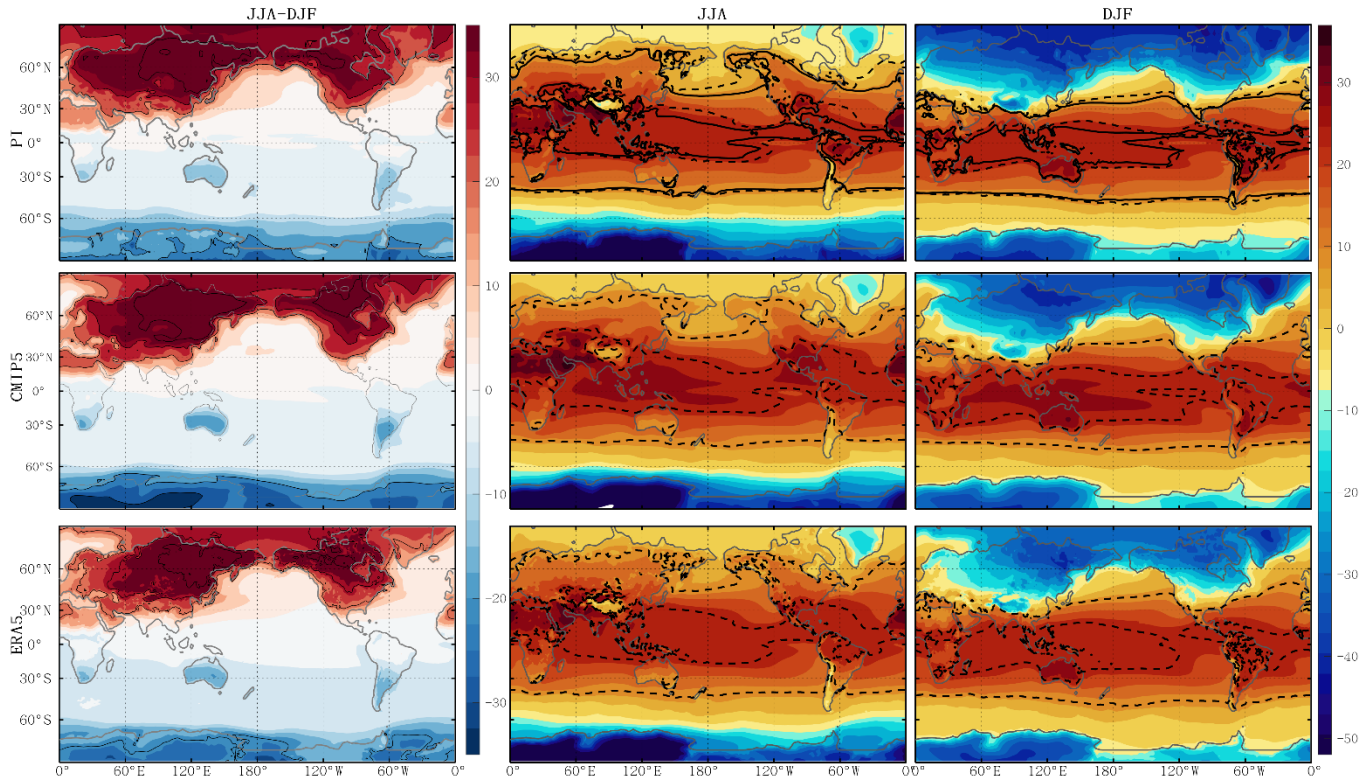

Figure S5. Compare the seasonal temperature change of the PI simulation with CMIP5 results and with the ERA5 re-analysis data for the period between 1940-1970. The CMIP5 data represent the multi-model mean from PI simulations of CESM, COSMOS, HadCM3, IPSL, MIROC, and GFDL models (data from DeepMIP). Contour lines in the middle and right columns indicate the 10 and 25 ℃ isotherms, with dashed and solid lines for ERA5 and PI in turn.

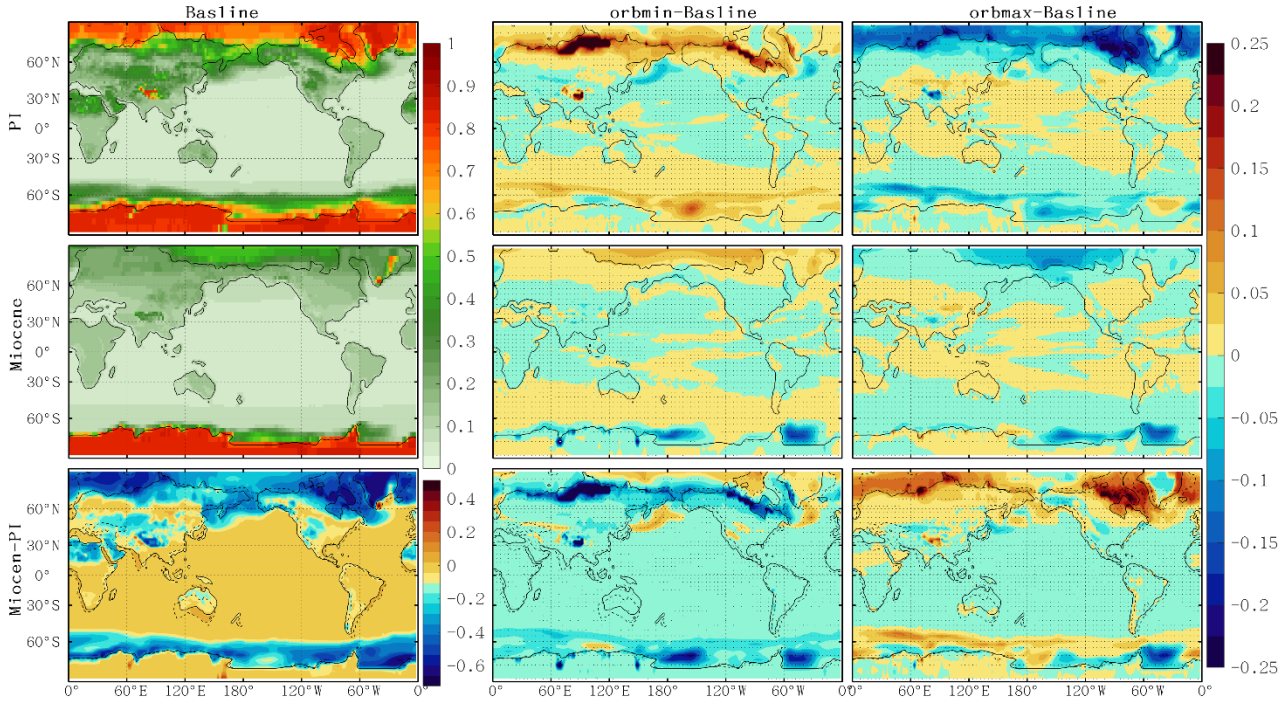

Figure S6. Surface albedo (left column) and its response to orbital insolation (right two columns), with the significance level of 95% denoted by dots.

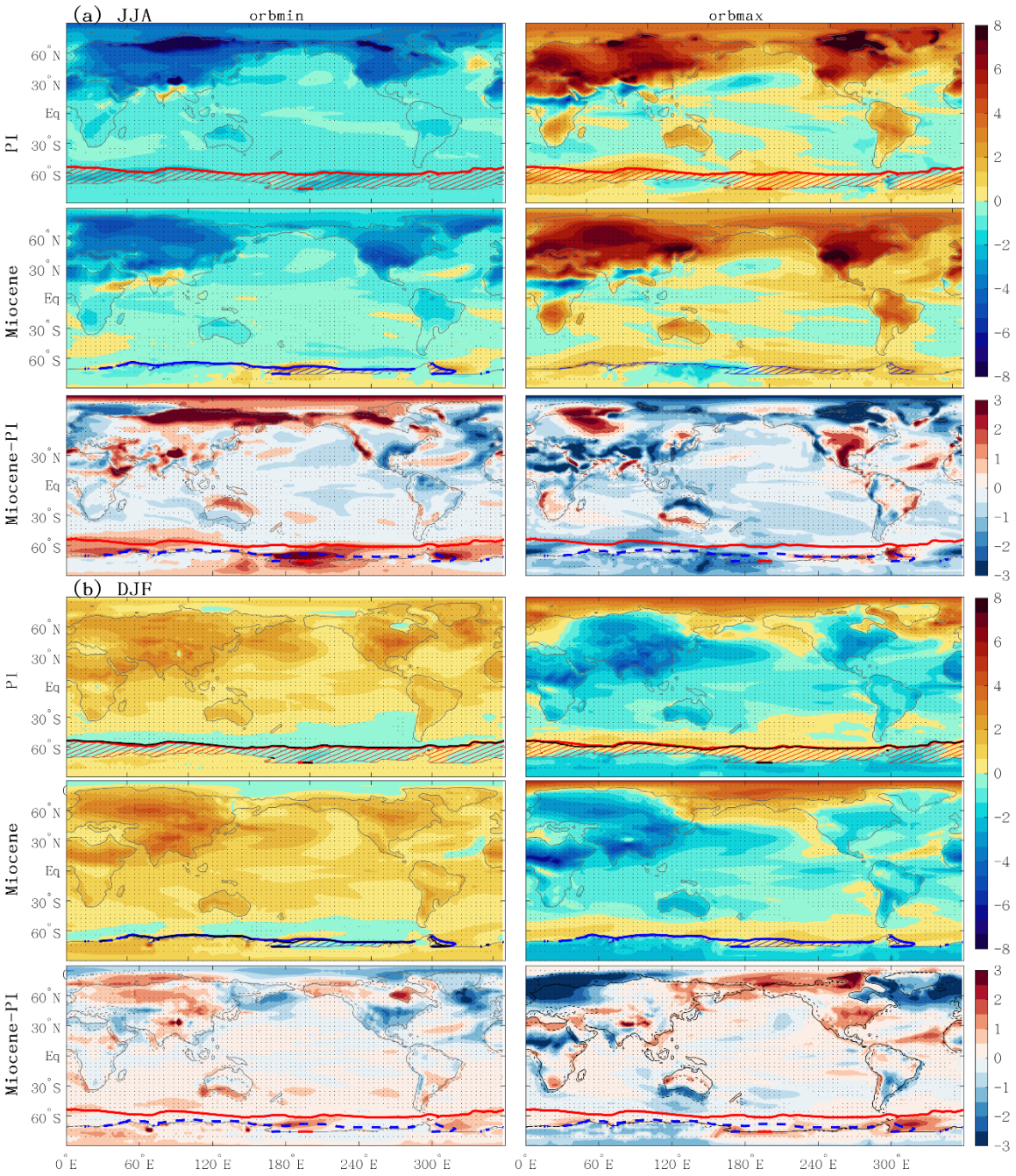

Figure S7. JJA (a) and DJF (b) temperature anomalies in the orbital simulations relative to the baseline and their differences between the PI and Miocene. Dots indicate the regions pass significance tests at 95% significance level. Hatching represents SH austral winter sea ice distribution in their baseline simulation.

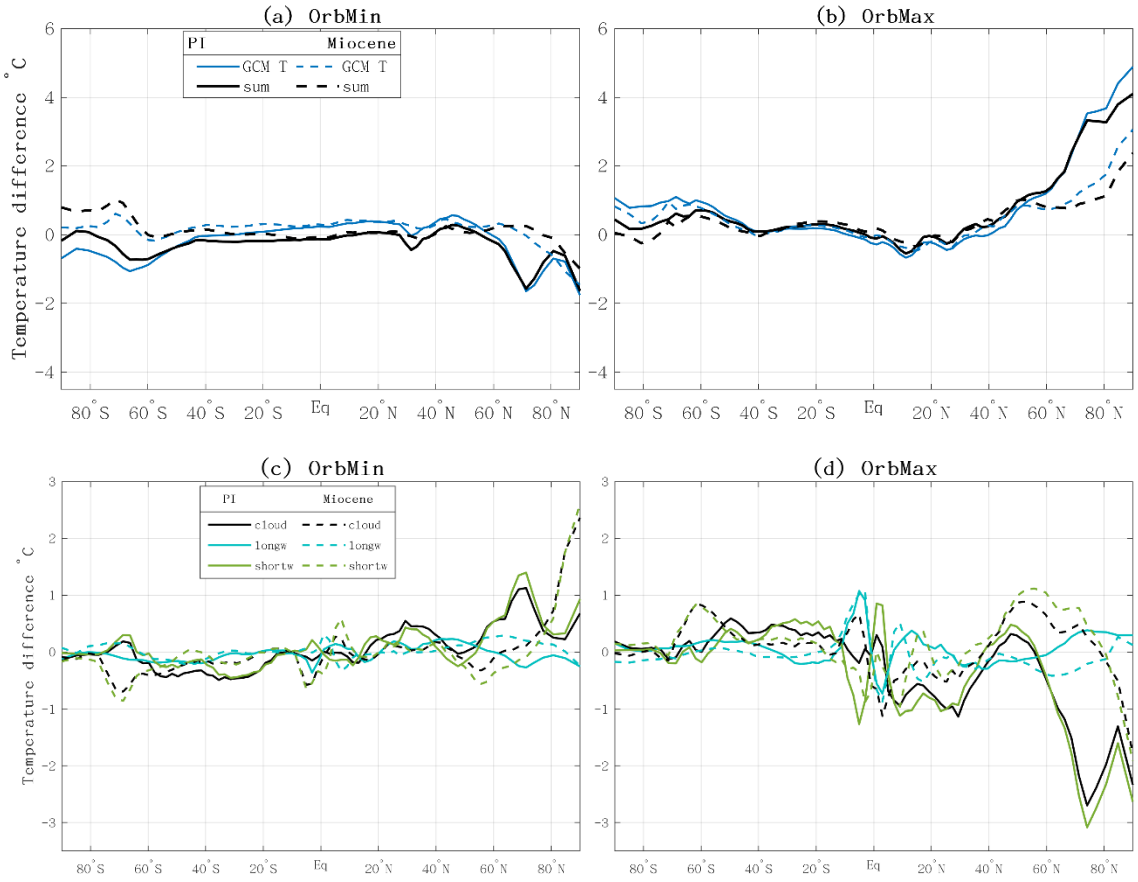

Figure S7. Comparison of the sum of EBA components with the GCM results for orbmin (a) and orbmax (b), and decomposition of cloud components into longwave and shortwave contributions for orbmin (c) and orbmax (d).

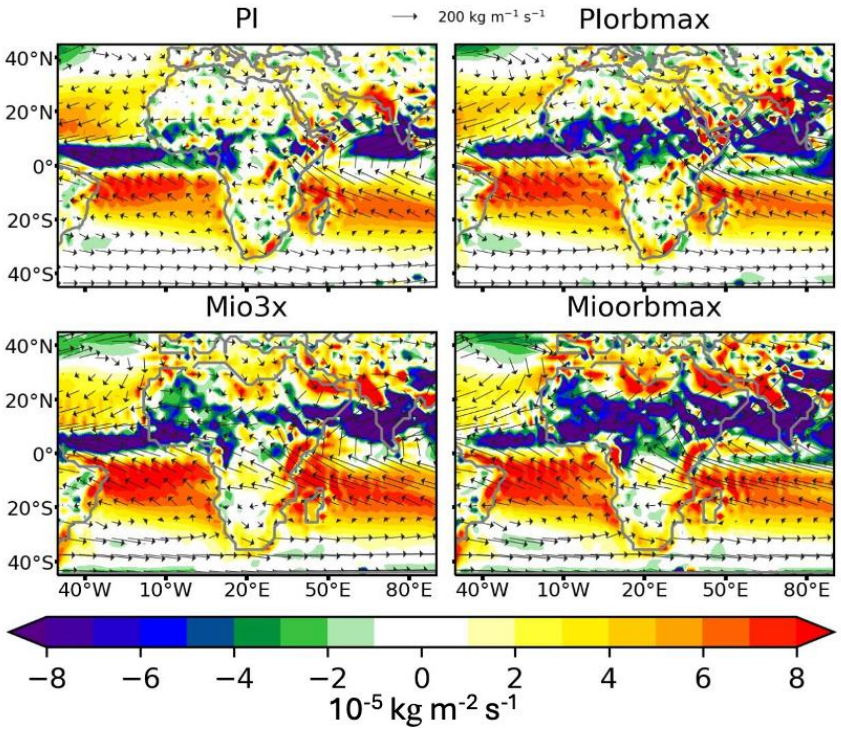

Figure S8. Divergence of water vapor flux (kg $m^{-2}s^{-1}$) and their response to orbital forcing over North Africa during summer.

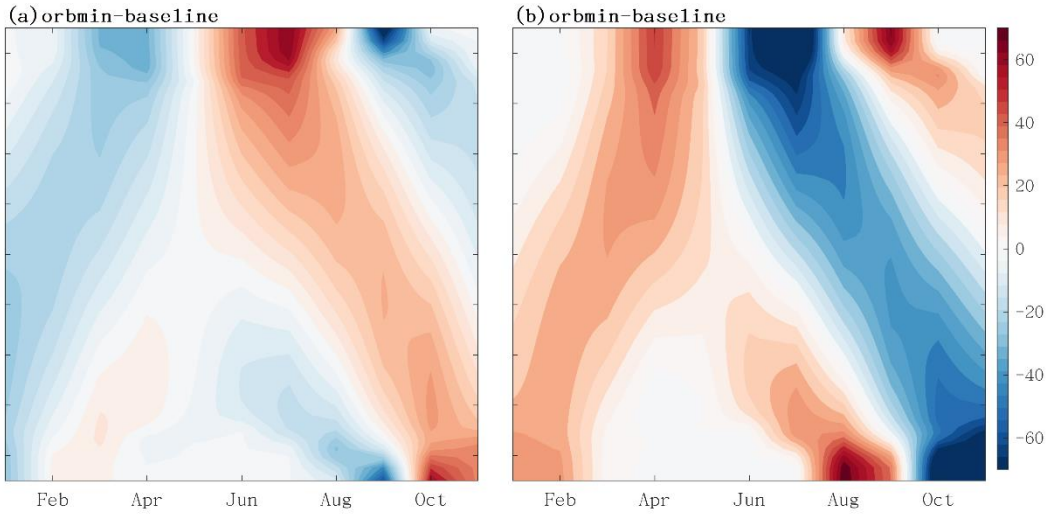

Figure S9. Monthly insolation change rate (W/m^2/month), representing the difference between the following month and that of the current month. High values are concentrated at north of 70 ℃N/S.

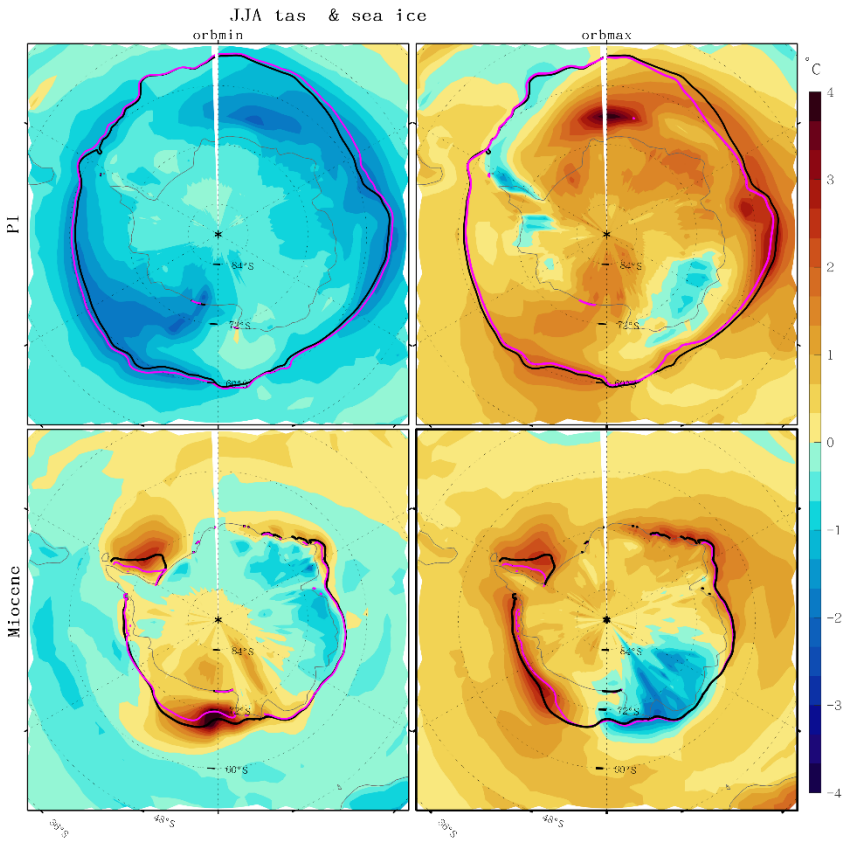

Figure S10. JJA surface air temperature anomalies (filled color) in the Southern Ocean and sea ice extent (solid lines). Black lines mark the baseline experiment sea ice, and magenta lines represent the simulated sea ice in the corresponding experiment.

Anthony, P. C., Mariana, V., and Robert, J.: A new flexible coupler for earth system modeling developed for CCSM4 and CESM1, The International Journal of High Performance Computing Applications, 26, 31-42, 10.1177/1094342011428141, 2011.

Davy, R. and Outten, S.: The Arctic Surface Climate in CMIP6: Status and Developments since CMIP5, Journal of Climate, 33, 8047-8068, 10.1175/jcli-d-19-0990.1, 2020.

Fan, X., Duan, Q., Shen, C., Wu, Y., and Xing, C.: Global surface air temperatures in CMIP6: historical performance and future changes, Environmental Research Letters, 15, 10.1088/1748-9326/abb051, 2020.

Gillett, N. P., Kirchmeier-Young, M., Ribes, A., Shiogama, H., Hegerl, G. C., Knutti, R., Gastineau, G., John, J. G., Li, L., Nazarenko, L., Rosenbloom, N., Seland, Ø., Wu, T., Yukimoto, S., and Ziehn, T.: Constraining human contributions to observed warming since the pre-industrial period, Nature Climate Change, 11, 207-212, 10.1038/s41558-020-00965-9, 2021.

Laskar, J. A. F. M. G. H. M.: La2010: a new orbital solution for the long-term motion of the Earth, Astronomy & Astrophysics, 532, A89 (2011), 10.1051/0004-6361/201116836, 2010.

Li, L. Y., Yongqiang, Tang, Y., Lin, P., Xie, J., Song, M., Dong, L., Zhou, T., Liu, L., Wang, L., Pu, Y., Chen, X., Chen, L., Xie, Z., Liu, H., Zhang, L., Huang, X., Feng, T., Zheng, W., Xia, K., Liu, H., Liu, J., Wang, Y., Wang, L., Jia, B., Xie, F., Wang, B., Zhao, S., Yu, Z., Zhao, B., and Wei, J.: The Flexible Global Ocean-Atmosphere-Land System Model Grid-Point Version 3 (FGOALS-g3): Description and Evaluation, Journal of Advances in Modeling Earth Systems, 12, 10.1029/2019ms002012, 2020.

Lin, P., Zhao, B., Wei, J., Liu, H., Zhang, W., Chen, X., Jiang, J., Ding, M., Man, W., Jiang, J., Zhang, X., Ding, Y., Bai, W., Jin, C., Yu, Z., Li, Y., Zheng, W., and Zhou, T.: The Super-large Ensemble Experiments of CAS FGOALS-g3, Advances in Atmospheric Sciences, 39, 1746-1765, 10.1007/s00376-022-1439-1, 2022.

Wang, Y., Yu, Z., Lin, P., Liu, H., Jin, J., Li, L., Tang, Y., Dong, L., Chen, K., Li, Y., Yang, Q., Ding, M., Meng, Y., Zhao, B., Wei, J., Ma, J., and Sun, Z.: FGOALS-g3 Model Datasets for CMIP6 Flux-Anomaly-Forced Model Intercomparison Project, Advances in Atmospheric Sciences, 37, 1093-1101, 10.1007/s00376-020-2045-8, 2020.

Wei, J., Liu, H., Zhao, Y., Lin, P., Yu, Z., Li, L., Xie, J., and Duan, A.: Simulation of the climate and ocean circulations in the Middle Miocene Climate Optimum by a coupled model FGOALS-g3, Palaeogeography, Palaeoclimatology, Palaeoecology, 617, 10.1016/j.palaeo.2023.111509, 2023.

Westerhold, T., Marwan, N., Drury, A. J., Liebrand, D., Agnini, C., Anagnostou, E., Barnet, J. S. K., Bohaty, S. M., De Vleeschouwer, D., Florindo, F., Frederichs, T., Hodell, D. A., Holbourn, A. E., Kroon, D., Lauretano, V., Littler, K., Lourens, L. J., Lyle, M., Pälike, H., Röhl, U., Tian, J., Wilkens, R. H., Wilson, P. A., and Zachos, J. C.: An astronomically dated record of Earth's climate and its predictability over the last 66 million years, 369, 1383-1387, doi:10.1126/science.aba6853, 2020.

Xie, Z., Wang, L., Wang, Y., Liu, B., Li, R., Xie, J., Zeng, Y., Liu, S., Gao, J., Chen, S., Jia, B., and Qin, P.: Land Surface Model CAS-LSM: Model Description and Evaluation, Journal of Advances in Modeling Earth Systems, 12, 10.1029/2020ms002339, 2020.

Zheng, W., Yu, Y., Luan, Y., Zhao, S., He, B., Dong, L., Song, M., Lin, P., and Liu, H.: CAS-FGOALS Datasets for the Two Interglacial Epochs of the Holocene and the Last Interglacial in PMIP4, Advances in Atmospheric Sciences, 37, 1034-1044, 10.1007/s00376-020-9290-8, 2020.